The University of Osaka
Institutional Knowledge Archive

| | |
|---|---|
| Title | Spatial control of skyrmion stabilization energy by low-energy $Ga^+$ ion implantation |
| Author(s) | Miki, S.; Hashimoto, K.; Cho, J. et al. |
| Citation | Applied Physics Letters. 2023, 122(20), p. 202401 |
| Version Type | VoR |
| URL | https://hdl.handle.net/11094/94756 |
| rights | This article may be downloaded for personal use only. Any other use requires prior permission of the author and AIP Publishing. This article appeared in Applied Physics Letters. 15 May 2023; 122, 202401 and may be found at https://doi.org/10.1063/5.0153768. |
| Note | |

*The University of Osaka Institutional Knowledge Archive : OUKA*

https://ir.library.osaka-u.ac.jp/

The University of Osaka

Applied Physics Letters

RESEARCH ARTICLE | MAY 15 2023

# Spatial control of skyrmion stabilization energy by low-energy $Ga^+$ ion implantation

S. Miki ; K. Hashimoto; J. Cho ; J. Jung ; C. Y. You ; R. Ishikawa ; E. Tamura; H. Nomura ; M. Goto ; Y. Suzuki

Check for updates

*Appl. Phys. Lett.* 122, 202401 (2023)
https://doi.org/10.1063/5.0153768

CHORUS

View Online
Export Citation
CrossMark

13 March 2024 09:22:49

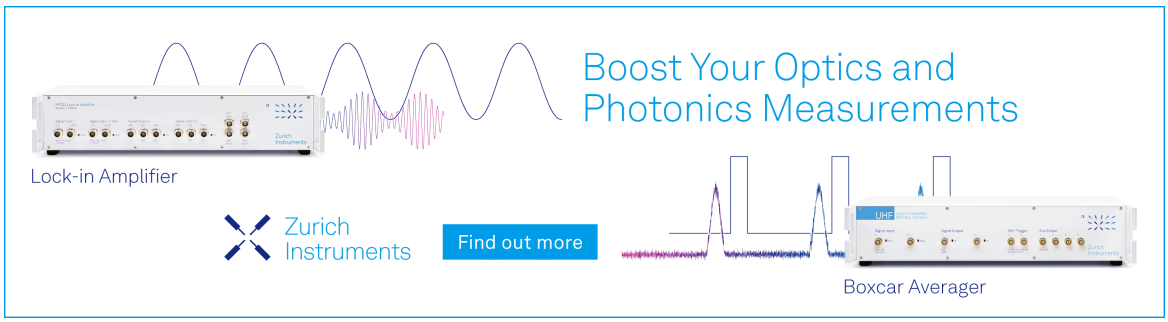


AIP Publishing

Applied Physics Letters ARTICLE pubs.aip.org/aip/apl

# Spatial control of skyrmion stabilization energy by low-energy $Ga^+$ ion implantation

Cite as: Appl. Phys. Lett. **122**, 202401 (2023); doi: 10.1063/5.0153768
Submitted: 11 April 2023 · Accepted: 2 May 2023 ·
Published Online: 15 May 2023

View Online Export Citation CrossMark

S. Miki,[1,2,3,a)] K. Hashimoto,[1,2,3] J. Cho,[4] J. Jung,[5] C. Y. You,[5] R. Ishikawa,[6] E. Tamura,[1,2,3] H. Nomura,[1,2,3] M. Goto,[1,2,3] and Y. Suzuki[1,2,3]

## AFFILIATIONS

[1]Graduate School of Engineering Science, Osaka University, Toyonaka, Osaka 560-8531, Japan
[2]Spintronics Research Network Division, Institute for Open and Transdisciplinary Research Initiatives, Osaka University, Suita, Osaka 565-0871, Japan
[3]Center for Spintronics Research Network (CSRN), Graduate School of Engineering Science, Osaka University, Toyonaka, Osaka 560-8531, Japan
[4]Division of Nanotechnology, Daegu Gyeongbuk Institute of Science and Technology (DGIST), Daegu 42988, South Korea
[5]Department of Physics and Chemistry, Daegu Gyeongbuk Institute of Science and Technology (DGIST), Daegu 42988, South Korea
[6]ULVAC-Osaka University Joint Research Laboratory for Future Technology, Osaka University, Suita, Osaka 565-0871, Japan

[a)]Author to whom correspondence should be addressed: miki@spin.mp.es.osaka-u.ac.jp

13 March 2024 09:22:49

## ABSTRACT

Magnetic skyrmions are candidates for information carriers in Brownian and stochastic computers. Developing a technique for fabricating a film with a suitable potential landscape, wherein the information carrier may diffuse freely, is essential for these probabilistic computers. In this study, to build the desired local potential into magnetic films, a 1.2 nm-thick Co-Fe-B film with a 5.2 nm-thick cap layer was irradiated by a focused ion beam (FIB) using $Ga^+$ as the ion source under a low acceleration voltage of 5 keV. The fluences ranged from 0 to $25 \times 10^{12}$ ions/cm$^2$. Consequently, the critical temperature at which skyrmions appear or disappear is shifted by several 1–10 K depending on the ion fluence. The origin of this effect is discussed by observing the ion implantation profile and the surface sputtering depth using time-of-flight secondary ion mass spectrometry (TOF-SIMS) and atomic force microscopy (AFM). The results of TOF-SIMS measurements show that most of the Ga atoms exist in the Co–Fe–B layer. If all Ga atoms exist in the Co–Fe–B layer, the Ga concentration is $7 \times 10^{-3}$ at. % after irradiation of $0.8 \times 10^{12}$ ions/cm$^2$. The AFM results show a sputtered pattern with 0.2 nm depth after irradiation of $16 \times 10^{12}$ ions/cm$^2$. Finally, the effect of irradiation on the diffusion coefficient was examined. It was determined that small fluences of $1.6 \times 10^{12}$ and $0.8 \times 10^{12}$ ions/cm$^2$ can construct a potential barrier controlling skyrmions while maintaining diffusion coefficients as high as 10 $\mu$m$^2$/s. The FIB process can be used to draw a circuit of probabilistic computers with skyrmions as information carriers.

*Published under an exclusive license by AIP Publishing.* https://doi.org/10.1063/5.0153768

A magnetic skyrmion is a particle-like spin texture characterized by a topological number.[1] The motion of the magnetic skyrmion can be driven by an electric current,[2–5] temperature gradient,[6,7] stochastic thermal torque,[8–14] and magnetic energy gradients.[15–18] Therefore, magnetic skyrmions are considered good candidates for information carriers in novel spintronics devices. In particular, the Brownian motion of a two-dimensional magnetic skyrmion embedded in a magnetic ultrathin film is suitable for realizing stochastic computer,[8] Brownian computer,[10,19,20] and cellular automatons,[13] which have been proposed and demonstrated as ultra-low power computers. In these unconventional computers, the confinement of skyrmions in circuits with an arbitrary landscape in the potential energy of the skyrmion is an essential technique. Several methods for fabricating circuits with local skyrmion potential energy differences have been demonstrated through the employment of additional deposition of a capping layer,[10,12,13] application of a local electric field,[9,15,21–23] and ion beam irradiation.[24–38]

Jibiki *et al.*[10] proposed the thickness of the $SiO_2$ capping layer (~0.2 nm) as a damage-free method to confine skyrmions. Moreover, this method ensures brisk Brownian motion of the skyrmion even after microfabrication.[10,12] However, it is unsuitable for creating a potential slope. In the ion beam irradiation method, the skyrmion energy can be continuously and locally controlled by locally changing the irradiation fluence.[30–38] Recently, using FIB irradiation, skyrmions


Published under an exclusive license by AIP Publishing

have been confined to 1D track.[33,35,38] The origin of the confinement has been discussed based on the observations of surface topography[32] and ion implantation.[25] However, a quantitative evaluation of the effect of ion irradiation on the diffusion coefficient has not yet been reported.

In this study, we aim to control the skyrmion stabilization energy locally to create and confine skyrmions via irradiating $Ga^+$ ions using the FIB machine. Subsequently, we investigate the effect of irradiation by sputtering the film surface and ion implantation into the sample. Furthermore, we discuss the degradation of the skyrmion diffusion in the irradiated region.

Sample A: Si/$SiO_2$ substrate | Ta(5.9) | Co–Fe–B(1.2) | Ta(0.22) | MgO(2.2) | $SiO_2$(2.9) (numbers in parentheses are the film thicknesses described in nanometer) and sample B, Si/$SiO_2$ substrate | Ta(5.9) | Co–Fe–B (1.2) | Ta(0.19) | MgO(2.2) | $SiO_2$(2.9), were deposited using a magnetron sputtering system (CANON ANELVA, E-880S-M) at 20 °C.[39] Each layer was sputtered using $Co_{16}Fe_{64}B_{20}$ (numbers represent the atomic percentages of the elements), MgO, $SiO_2$ compositional targets, and a metallic Ta target in an Ar atmosphere. Sample A was annealed at 200 °C for 1 h after the deposition of all layers, while sample B was not annealed to enhance the diffusion coefficient of the skyrmion.[10,12] In the non-annealed sample, the Co–Fe–B layer is in an amorphous state.[40] The annealing at 200 °C results in partial crystallization of the Co–Fe–B layer[40] and a reduction in the diffusion coefficient.[10] Subsequently, the samples were irradiated with $Ga^+$-source FIB using a scanning electron microscope (SEM) (FEI, Versa 3D Dual Beam). An accelerating voltage of 5 keV and a beam current of 1.3 pA (the lowest voltage and current of the machine) were employed to avoid sputtering of the film and stop the $Ga^+$ ions in the Co–Fe–B layer. Thereafter, to evaluate the aging effect following the irradiation, the samples with 8 months of aging (samples A and B) and samples without aging (7–11 days after irradiation) (samples A′ and B′) were investigated. The skyrmions are observed using a polar-magneto-optical Kerr effect (p-MOKE) microscope at various temperatures under a perpendicular bias magnetic field. The observed sizes of the skyrmions are ranged as 0.5–2 $\mu$m. Because a skyrmion of this size is stabilized by the magnetic dipole interaction energy, it is called a "skyrmion bubble."[41] The surface morphology after ion irradiation was observed using atomic force microscope (AFM) (Hitachi High-Tech, AFM5300E). The implantation depth profile was observed using a time-of-flight secondary ion mass spectrometer (TOF-SIMS) (ION-TOF, TOF.SIMS5).

The p-MOKE images of sample B (without annealing/aging for 8 months) at (a) 338 and (b) 345 K under the application of external magnetic field $H = -0.41$ mT around the region of the irradiation of $0.8 \times 10^{12}$ ions/cm$^2$ are shown in Fig. 1 (see the supplementary material Videos S1 and S2). In Fig. 1(a), skyrmions appear exclusively in the non-irradiated region. In contrast, in Fig. 1(b), they appear in the irradiated region, and those outside the irradiated region reduce in size. The results clearly demonstrate the control of skyrmion stabilization energy by ion irradiation. Figures 1(c) and 1(d) show the hysteresis curves obtained for the same sample. The hysteresis curves were evaluated from the MOKE images at (c) 338 and (d) 345 K. The black and red points represent the ratio of the black to the white domain

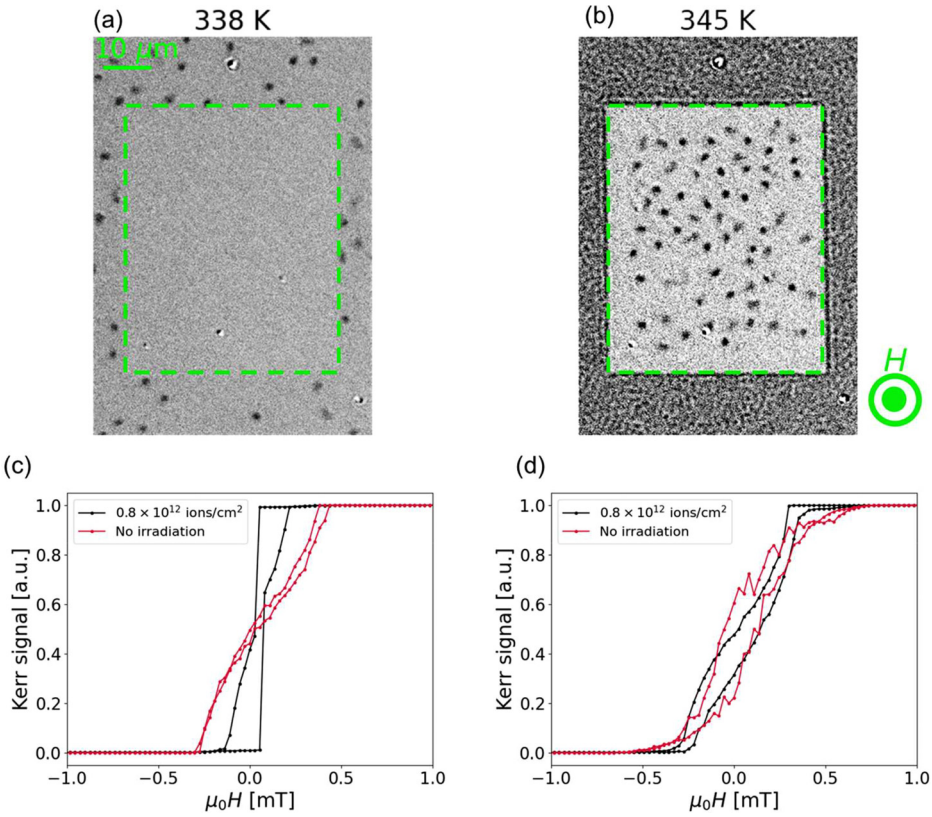


**FIG. 1.** Magneto-optical Kerr effect (MOKE) microscope observation of sample B (without annealing/aged for 8 months). (a) and (b) MOKE images captured under an external field of −0.41 mT at (a) 338 and (b) 345 K, respectively. The rectangular region in the center of the image is the area where the film is irradiated by the FIB. The fluence is $0.8 \times 10^{12}$ ions/cm$^2$. (c) and (d) Hysteresis curves observed by MOKE microscope at (c) 338 and (d) 345 K, respectively. Black plots and curves indicate the results measured in the irradiated region for fluence of $0.8 \times 10^{12}$ ions/cm$^2$ and the red plots and curves indicate the results in the non-irradiated region.

13 March 2024 09:22:49


Published under an exclusive license by AIP Publishing

areas in the irradiated and non-irradiated regions, respectively. The hysteresis curves show the reductions in the $Q$-factors [relative size of the perpendicular magnetic anisotropy (PMA) energy to the demagnetizing energy] at higher temperatures. This is a typical tendency because PMA decreases faster than the demagnetization energy with the increase in the temperature. The hysteresis curves also show that the $Q$-factor is enhanced by the ion irradiation of $0.8 \times 10^{12}$ ions/cm$^2$. Furthermore, the saturation magnetic field $H_s$ increases by a factor of approximately 1/2 with the irradiation, i.e., effective PMA increases approximately twice with irradiation (see the supplementary material S3). Therefore, a considerable increase in the effective PMA owing to a small amount of irradiation ($0.8 \times 10^{12}$ ions/cm$^2$) contributes to the enhancement in the $Q$-factor.

Figures 2(a) and 2(b) show the phase diagrams of the skyrmions in sample A (with annealing/aging for 8 months) and B (without annealing/aging for 8 months), respectively. The horizontal and vertical axes represent the ion fluence and measurement temperature, respectively. The observation was performed using a MOKE microscope under a perpendicular external magnetic field of $-0.41$ mT. The black and red plots indicate the creation and annihilation temperatures of the skyrmion, respectively. Furthermore, the solid curves show the interpolation by spline fitting. The plots and solid curves show the results of the *aged* samples, which were irradiated approximately eight months prior to performing the measurement. Regions with different colors represent different phases. In the sepia-colored region, magnetization is preferentially in-plane (IP). The skyrmion phase (SK) is stable in the yellow-colored region. In contrast, in the sky blue region, a uniform out-of-plane magnetization state (OOP) or maze domain (MD) is stable. In both cases, the skyrmion phase appears only in a narrow temperature range (approximately 5 K) between the OOP/MD and IP phases.

As shown in Fig. 1, the $Q$-factor is smaller at higher temperatures. Therefore, the film exhibits OOP/MD and IP in the lower- and higher-temperature regions, respectively. However, in between, a skyrmion phase appeared. The energy of the straight DMI domain wall is expressed as $E = 4\sqrt{A_{\mathrm{ex}} K_{\mathrm{u,\,eff}}} - \pi E_{\mathrm{DMI}} - E_{\mathrm{Dipole}}$.[41,42] Here, $A_{\mathrm{ex}}$, $E_{\mathrm{DMI}}$, and $E_{\mathrm{Dipole}}$ are the exchange stiffness constant, interfacial Dzyaloshinskii–Moriya interaction ($i$-DMI) energy, and dipole energy, respectively. Furthermore, $K_{\mathrm{u,\,eff}} = K_{\mathrm{u}}(1 - Q^{-1})$ is the effective perpendicular anisotropy energy. The skyrmion is stabilized by the $i$-DMI and/or dipole energies when the DMI and demagnetization energies are balanced ($Q = 1$). Therefore, the narrow temperature range of the skyrmion phase in our experiment is because of the small size of $i$-DMI and dipole energy in our system ($i$-DMI is smaller than $-0.04 \pm 0.03$ mJ/m$^2$ in pristine samples, see the supplementary material S4). Moreover, in our experiments, the skyrmions in the Ta | Co–Fe–B | Ta film exhibit (i) enhancement of the diffusion coefficient in the 1D system and (ii) gyro-diffusion.[12,43] Therefore, the observed magnetic bubbles are classified as skyrmions with a definite skyrmion number. A larger $i$-DMI is expected to expand the temperature range of the skyrmion phase as the previous studies about altering $i$-DMI by ion irradiation.[26,28,29,33,36,37]

In Fig. 2, the phase boundaries for samples A′ and B′ without aging (11 days after ion irradiation) are indicated by dashed curves. The aging effect appears with the increase in the critical temperature and is significant for films with larger ion fluences. The 8 month-aging does not cause a change in the critical temperature of the samples without irradiation (ion-fluence = 0); however, it does affect the films with non-zero ion fluence. The effect of aging is considered to be related to the relaxation of atom positions after ion irradiation. In real applications, the sample should be annealed at an appropriate temperature after ion implantation to avoid the aging effect.

Identifying the mechanism to change the critical temperature by ion irradiation is difficult because the skyrmion phase is stabilized by a delicate balance between the magnetic energies. Therefore, in the following, we only attempt to gather circumstantial evidence.

Figure 3 shows the $Ga^+$ implantation profile measured by TOF-SIMS. The primary and etching ion beam sources are Bi and $O_2$, respectively. The $x$ axis represents the sputtering depth converted from the sputtering time, assuming that the half-value width of the Fe peak is 1.2 nm. It should be noted that because of the different sputtering rates and knocking-on processes, the scale is not correct for different elements. The $y$ axis represents the count of the detected secondary ions. The ion count is dependent on the matrix element (matrix effect). Therefore, the ion counts in different matrices cannot be directly compared. Figures 3(a) and 3(b) show the depth profiles of sample A with and without the FIB irradiation, respectively (the profiles of each element are shown in the supplementary material S5).

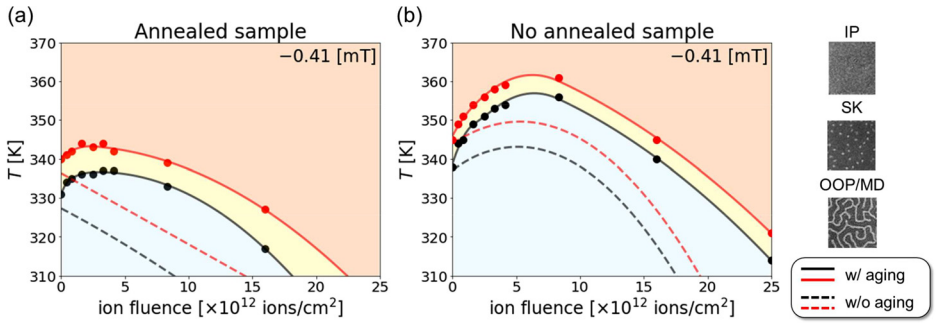


**FIG. 2.** Phase diagrams of the skyrmion film under the external magnetic field of $-0.41$ mT in (a) sample A (with annealing/aged for 8 months) and (b) sample B (without annealing/aged for 8 months). $x$ and $y$ axes indicate the ion fluence and measurement temperature, respectively. Plots indicate the creation (black) and annihilation (red) temperature of the skyrmions. The solid curves show the interpolation via the spline fitting. Red, yellow, and blue painted regions indicate the in-plane (IP) magnetization, skyrmion phase (SK), and out-of-plane (OOP) magnetization or maze domain (MD) state, respectively. The dashed lines indicate the phase boundary in samples A′ (with annealing/aged for 11 days) and B′ (without annealing/aged for 11 days).

13 March 2024 09:22:49


Published under an exclusive license by AIP Publishing

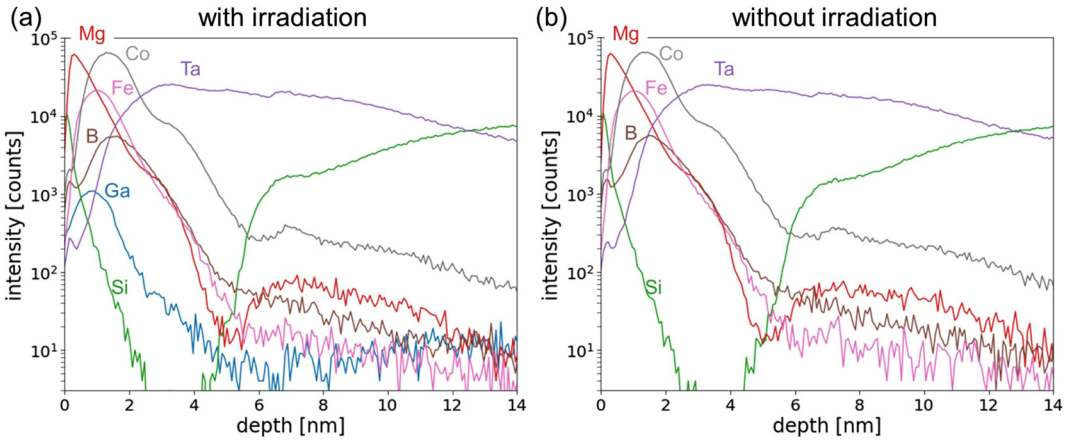


**FIG. 3.** Depth profile of the film measured by the time-of-flight secondary ion mass spectroscopy (TOF-SIMS). (a) Depth profile of sample B′ (with annealing/one week after ion irradiation) after FIB irradiation of $0.8 \times 10^{12}$ ions/cm$^2$. (b) Depth profile of the sample without FIB irradiation. The depth is scaled using the Fe milling rate.

The ion fluence is $0.8 \times 10^{12}$ ions/cm$^2$. The two profiles are almost identical except for Ga, with a faint trace of the knock-on process. $Ga^+$ ions are detected only in the sample subjected to the FIB irradiation. As indicated by the profile, most of the $Ga^+$ ions are certainly doped into the Co–Fe–B layer. In order to verify the reliability of the experiment, an ion-doping simulation called stopping range in matter (SRIM)[44] is conducted (see the supplementary material S6 on the discussion of the effect of low ion acceleration voltage). The parameters used are the same as those used in our experiment and there are no adjustment parameters. The simulation shows that most of the Ga ions (approximately 30%) stop in the Co–Fe–B layer. This result is in agreement with our observation (an increase in Ga-ion count in the Si layer should be a matrix effect). For the extreme case where all ions are implanted into the Co–Fe–B layer, the relative concentration of Ga ions to the Co–Fe–B host atoms reaches $7 \times 10^{-3}$ at% for an irradiation fluence of $0.8 \times 10^{12}$ ions/cm$^2$. Thus, the concentration seems to be considered to modulate the skyrmion stabilization energy.

We also performed atomic force microscopy (AFM) measurements to verify sputtering of atoms from the sample (see the supplementary material S7 presents further detail). However, the milling depth resulting from the ion irradiation of $16 \times 10^{12}$ ions/cm$^2$ is approximately 0.2 nm, i.e., 1 atomic layer. The effect of milling the surface corresponds to a 0.2–1.0 K change in the critical temperature.[10] Therefore, sputtering exerts a minor effect throughout our experiment.

As aforedescribed, the main mechanism to change the skyrmion stabilization energy is expected to be Ga implantation, which may result in the reduction of the demagnetization, PMA, exchange, and *i*-DMI energies. Based on the reduction of all energy scales, the reduction in the critical temperature for a large fluence region can be explained. However, in the small-fluence region, the critical temperature increases with an increase in the ion fluence. This result is consistent with the observation in Fig. 1, where a small amount of ion-irradiation ($0.8 \times 10^{12}$ ions/cm$^2$) increases the PMA. Anisotropic lattice strain and rearrangement of atoms that are introduced by the implantation seem to be adequate causes for it (see the supplementary material S3). Microscopic parameters, such as changes in the atomic distance, coordination number, and preferential bond direction, should be considered to clarify how a small fluence can provide such different behavior. Microscopic measurements, such as XAFS experiments, are required to further investigate this aspect.

Finally, we investigate the effect of irradiation on the Brownian motion of skyrmions, as shown in Fig. 4. Because the lifetime of the skyrmions in sample A (annealing/aged for 8 months) is exceedingly short to obtain a reliable diffusion coefficient, sample B (without annealing/aged for 8 months), with fewer skyrmion trapping sites was used in this experiment. Figure 4(a) presents the mean squared displacement (MSD) in and outside the irradiated region at 338 and 345 K, respectively (black triangles and red circles, respectively). The irradiation fluence shown by the black triangle plots is $0.8 \times 10^{12}$ ions/cm$^2$. The fluence is relatively small but sufficiently large to confine the skyrmion in the irradiated area, as shown in Fig. 1. The MSD is described by the ensemble average of the square displacements of the skyrmions, and the diffusion coefficient $D$ is obtained from the MSD as follows:

$$\mathrm{MSD} = \lim_{t\to\infty} \left\langle \left(\mathbf{x}(t+\Delta t) - \mathbf{x}(t)\right)\cdot\left(\mathbf{x}(t+\Delta t) - \mathbf{x}(t)\right)\right\rangle = 4D\Delta t, \tag{1}$$

where $\Delta t$ is the elapsed time from time $t$. The time step is set to 6 ms. The diffusion coefficients shown in Fig. 4(a) are 4.6 and 4.8 $\mu$m$^2$/s for the irradiated and non-irradiated samples. Even after ion irradiation, a comparable diffusion coefficient is obtained, although the temperature ranges are different. In Fig. 4(b), the temperature dependence of the diffusion coefficients is shown. Blue-inverted- and black-triangle plots are the diffusion coefficients of the irradiated sample, $1.6 \times 10^{12}$ and $0.8 \times 10^{12}$ ions/cm$^2$, respectively, and red circles are those of the non-irradiated sample. In the irradiated sample, skyrmions appear at higher temperatures. The observed maximum diffusion coefficients are greater than 10 $\mu$m$^2$/s in both cases. The dashed lines in Fig. 4(b) are those fitted to the experimental results. As for skyrmion diffusion, the hopping diffusion between defects in the sample is dominant.[8,9] Therefore, the activation energies of hopping diffusion can be obtained from the slopes of the fitted lines, which are 5.91 eV ($1.6 \times 10^{12}$ ions/cm$^2$) and 6.17 eV ($0.8 \times 10^{12}$ ions/cm$^2$) for the irradiated samples and 6.32 eV for the non-irradiated samples. Surprisingly, ion irradiation does not

13 March 2024 09:22:49


Published under an exclusive license by AIP Publishing

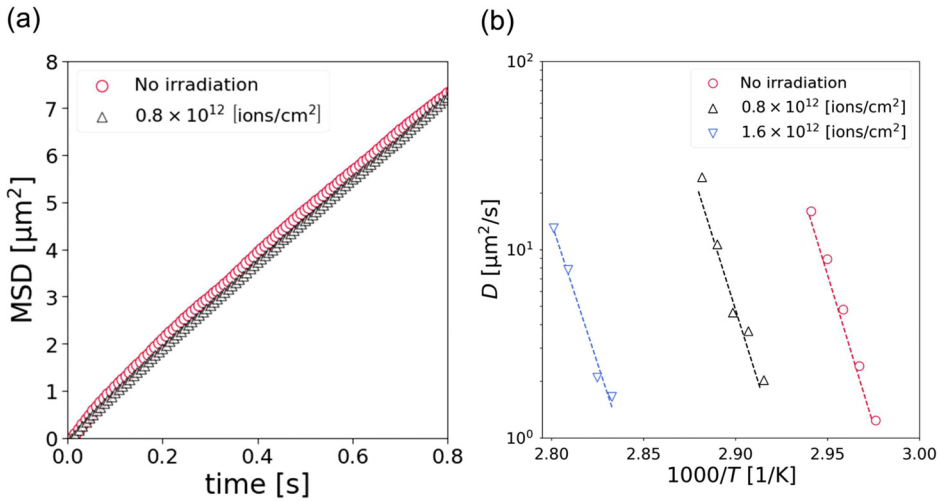


**FIG. 4.** Diffusion of the skyrmions in sample B (without annealing/aged for 8 months). (a) Mean squared displacement (MSD) in and out of the FIB irradiated region. Black-triangle plots show the MSD for the sample with irradiation. The measurement was performed at 338 K. Red-circle plots are for the sample without irradiation. The measurement was performed at 345 K. (b) Temperature dependence of the diffusion coefficient. The blue-inverted-triangle plots represent the diffusion coefficient for the sample with ion irradiation of $1.6 \times 10^{12}$ ions/cm$^2$. The black-triangle plots are for the sample with ion irradiation of $0.8 \times 10^{12}$ ions/cm$^2$. Furthermore, the red-circle plots are for the non-irradiated sample. The dashed lines represent the fitted lines.

change the activation energy. Therefore, small irradiation fluences do not affect diffusion. Here, we found a condition to confine the skyrmion while maintaining a high diffusion coefficient. A larger amount of irradiation reduces the diffusion coefficient (approximately 1 $\mu$m$^2$/s for a sample with $25 \times 10^{12}$ ions/cm$^2$ fluence). However, the optimum fluence to obtain the highest diffusion coefficient could not be determined because of the limitation in the camera frame speed (130 frame/s), which limits the measurement of a large diffusion coefficient (larger than 30 $\mu$m$^2$/s).

In summary, we investigated the effects of $Ga^+$-source FIB irradiation on skyrmion films. The film stacking is Ta|Co-Fe-B|Ta|MgO|$SiO_2$. The low-energy (5 keV) FIB irradiation affects the magnetic properties and facilitates precise control of the critical temperatures in a wide range from a few kelvins to several tens of kelvins. Particularly, small fluence irradiation ($1.6 \times 10^{12}$ and $0.8 \times 10^{12}$ ions/cm$^2$) on the non-annealed sample made confinement of the skyrmion possible while maintaining a high diffusion coefficient (as high as 10 $\mu$m$^2$/s). Furthermore, the FIB irradiation does not change the activation energy of diffusion. The results of this work can be applied to construct an arbitrarily shaped potential landscape necessary for realizing future skyrmion circuits.

See the supplementary material for (S1) video of the skyrmions in the non-irradiated region; (S2) video of the skyrmions in the irradiated region; (S3) temperature dependence of the saturated magnetic field; (S4) Brillouin light scattering measurement to obtain the *i*-DMI energy density; (S5) profiles of each element obtained via the TOF-SIMS measurement; and (S6) SRIM simulation to discuss the effect of the acceleration voltage; and (S7) AFM measurements.

This research and development work was supported by ULVAC, Inc., JSPS Grant-in-Aid for Scientific Research (S) (Grant No. JP20H05666), Japan and CREST (No. JPMJCR20C1) of the Japan Science and Technology Agency, Nanotechnology Platform of MEXT (Grant No. JPMXP09 S-21-OS-0053), and the National Research Foundation of Korea (Grant No. 2021M3F3A2A01037525). The research was also supported by the Center for Spintronics Research Network (CSRN), Graduate School of Engineering Science, Osaka University.

## AUTHOR DECLARATIONS

### Conflict of Interest

The authors have no conflicts to disclose.

### Author Contributions

**Soma Miki:** Conceptualization (lead); Data curation (lead); Formal analysis (lead); Investigation (lead); Methodology (lead); Software (lead); Validation (lead); Visualization (lead); Writing – original draft (lead); Writing – review & editing (lead). **Yoshishige Suzuki:** Funding acquisition (lead); Project administration (lead); Resources (lead); Supervision (lead); Writing – review & editing (equal). **Ken Hashimoto:** Investigation (equal). **Jaehun Cho:** Investigation (equal). **Jinyong Jung:** Investigation (equal). **Chun-Yeol You:** Investigation (equal). **Ryo Ishikawa:** Data curation (equal); Investigation (supporting). **Eiiti Tamura:** Data curation (supporting); Formal analysis (supporting); Writing – review & editing (equal). **Hikaru Nomura:** Investigation (supporting); Software (supporting). **Minori Goto:** Supervision (equal).

## DATA AVAILABILITY

The data that support the findings of this study are available from the corresponding author upon reasonable request.

## REFERENCES

[1]N. Nagaosa and Y. Tokura, Nat. Nanotechnol. **8**, 899 (2013).

13 March 2024 09:22:49


Published under an exclusive license by AIP Publishing

[2]F. Jonietz, S. Mühlbauer, C. Pfleiderer, A. Neubauer, W. Münzer, A. Bauer, T. Adams, R. Georgii, P. Böni, R. A. Duine, K. Everschor, M. Garst, and A. Rosch, Science **330**, 1648 (2010).
[3]S. Woo, K. Litzius, B. Krüger, M.-Y. Im, L. Caretta, K. Richter, M. Mann, A. Krone, R. M. Reeve, M. Weigand, P. Agrawal, I. Lemesh, M.-A. Mawass, P. Fischer, M. Kläui, and G. S. D. Beach, Nat. Mater. **15**, 501 (2016).
[4]W. Jiang, X. Zhang, G. Yu, W. Zhang, X. Wang, M. Benjamin Jungfleisch, J. E. Pearson, X. Cheng, O. Heinonen, K. L. Wang, Y. Zhou, A. Hoffmann, and S. G. E. te Velthuis, Nat. Phys. **13**, 162 (2017).
[5]T. Dohi, S. DuttaGupta, S. Fukami, and H. Ohno, Nat. Commun. **10**, 5153 (2019).
[6]M. Mochizuki, X. Z. Yu, S. Seki, N. Kanazawa, W. Koshibae, J. Zang, M. Mostovoy, Y. Tokura, and N. Nagaosa, Nat. Mater. **13**, 241 (2014).
[7]R. Iguchi, S. Kasai, K. Koshikawa, N. Chinone, S. Suzuki, and K.-I. Uchida, Sci. Rep. **9**, 18443 (2019).
[8]J. Zázvorka, F. Jakobs, D. Heinze, N. Keil, S. Kromin, S. Jaiswal, K. Litzius, G. Jakob, P. Virnau, D. Pinna, K. Everschor-Sitte, L. Rózsa, A. Donges, U. Nowak, and M. Kläui, Nat. Nanotechnol. **14**, 658 (2019).
[9]T. Nozaki, Y. Jibiki, M. Goto, E. Tamura, T. Nozaki, H. Kubota, A. Fukushima, S. Yuasa, and Y. Suzuki, Appl. Phys. Lett. **114**, 012402 (2019).
[10]Y. Jibiki, M. Goto, E. Tamura, J. Cho, S. Miki, R. Ishikawa, H. Nomura, T. Srivastava, W. Lim, S. Auffret, C. Baraduc, H. Bea, and Y. Suzuki, Appl. Phys. Lett. **117**, 082402 (2020).
[11]L. Zhao, Z. Wang, X. Zhang, X. Liang, J. Xia, K. Wu, H.-A. Zhou, Y. Dong, G. Yu, K. L. Wang, X. Liu, Y. Zhou, and W. Jiang, Phys. Rev. Lett. **125**, 27206 (2020).
[12]S. Miki, Y. Jibiki, E. Tamura, M. Goto, M. Oogane, J. Cho, R. Ishikawa, H. Nomura, and Y. Suzuki, J. Phys. Soc. Jpn. **90**, 083601 (2021).
[13]R. Ishikawa, M. Goto, H. Nomura, and Y. Suzuki, Appl. Phys. Lett. **119**, 072402 (2021).
[14]M. Goto, H. Nomura, and Y. Suzuki, J. Magn. Magn. Mater. **536**, 167974 (2021).
[15]H. Xia, C. Song, C. Jin, J. Wang, J. Wang, and Q. Liu, J. Magn. Magn. Mater. **458**, 57 (2018).
[16]E. Tamura, C. Liu, S. Miki, J. Cho, H. Nomura, M. Goto, R. Nakatani, and Y. Suzuki, arXiv:2005.04860 (2020).
[17]J. Cho, E. Tamura, C. Liu, S. Miki, C.-Y. You, J.-S. Kim, H. Nomura, M. Goto, R. Nakatani, and Y. Suzuki, New J. Phys. **22**, 103053 (2020).
[18]S. Miki, E. Tamura, H. Nomura, M. Goto, and Y. Suzuki, J. Phys. Soc. Jpn. **90**, 114703 (2021).
[19]F. Peper, J. Lee, J. Carmona, J. Cortadella, and K. Morita, J. Emerg. Technol. Comput. Syst. **9**(1), 1 (2013).
[20]L.-J. Fei, J. Lee, X. Huang, and F. Peper, Physica D **428**, 133052 (2021).
[21]M. Schott, A. Bernand-Mantel, L. Ranno, S. Pizzini, J. Vogel, H. Béa, C. Baraduc, S. Auffret, G. Gaudin, and D. Givord, Nano Lett. **17**, 3006–3012 (2017).
[22]C. Ma, X. Zhang, J. Xia, M. Ezawa, W. Jiang, T. Ono, S. N. Piramanayagam, A. Morisako, Y. Zhou, and X. Liu, Nano Lett. **19**, 353–361 (2019).
[23]R. Ishikawa, M. Goto, H. Nomura, and Y. Suzuki, Appl. Phys. Lett. **121**, 252402 (2022).
[24]S. Blomeier, D. McGrouther, R. O'Neill, S. McVitie, J. N. Chapman, M. C. Weber, B. Hillebrands, and J. Fassbender, J. Magn. Magn. Mater. **290–291**, 731 (2005).
[25]L. Herrera Diez, F. García-Sánchez, J.-P. Adam, T. Devolder, S. Eimer, M. S. El Hadri, A. Lamperti, R. Mantovan, B. Ocker, and D. Ravelosona, Appl. Phys. Lett. **107**, 032401 (2015).
[26]X. Zhao, B. Zhang, N. Vernier, X. Zhang, M. Sall, T. Xing, L. H. Diez, C. Hepburn, L. Wang, G. Durin, A. Casiraghi, M. Belmeguenai, Y. Roussigné, A. Stashkevich, S. M. Chérif, J. Langer, B. Ocker, S. Jaiswal, G. Jakob, M. Kläui, W. Zhao, and D. Ravelosona, Appl. Phys. Lett. **115**, 122404 (2019).
[27]S. Mendisch, F. Riente, V. Ahrens, L. Gnoli, M. Haider, M. Opel, M. Kiechle, M. Ruo Roch, and M. Becherer, Phys. Rev. Appl. **16**, 014039 (2021).
[28]M. C. H. de Jong, M. J. Meijer, J. Lucassen, J. van Liempt, H. J. M. Swagten, B. Koopmans, and R. Lavrijsen, Phys. Rev. B **105**, 064429 (2022).
[29]H. T. Nembach, E. Jué, K. Poetzger, J. Fassbender, T. J. Silva, and J. M. Shaw, J. Appl. Phys. **131**, 143901 (2022).
[30]F. C. Ummelen, T. Lichtenberg, H. J. M. Swagten, and B. Koopmans, Appl. Phys. Lett. **115**, 102402 (2019).
[31]K. Fallon, S. Hughes, K. Zeissler, W. Legrand, F. Ajejas, D. Maccariello, S. McFadzean, W. Smith, D. McGrouther, S. Collin, N. Reyren, V. Cros, C. H. Marrows, and S. McVitie, Small **16**, e1907450 (2020).
[32]V. Ahrens, S. Mendisch, W. Kaiser, M. Kiechle, S. B.-v. Breitkreutz-v. Gamm, and M. Becherer, J. Magn. Magn. Mater. **523**, 167591 (2021).
[33]R. Juge, K. Bairagi, K. G. Rana, J. Vogel, M. Sall, D. Mailly, V. T. Pham, Q. Zhang, N. Sisodia, M. Foerster, L. Aballe, M. Belmeguenai, Y. Roussigné, S. Auffret, L. D. Buda-Prejbeanu, G. Gaudin, D. Ravelosona, and O. Boulle, Nano Lett. **21**, 2989–2996 (2021).
[34]V. Ahrens, L. Gnoli, D. Giuliano, S. Mendisch, M. Kiechle, F. Riente, and M. Becherer, AIP Adv. **12**, 035325 (2022).
[35]L. M. Kern, B. Pfau, V. Deinhart, M. Schneider, C. Klose, K. Gerlinger, S. Wittrock, D. Engel, I. Will, C. M. Günther, R. Liefferink, J. H. Mentink, S. Wintz, M. Weigand, M. J. Huang, R. Battistelli, D. Metternich, F. Büttner, K. Höflich, and S. Eisebitt, Nano Lett. **22**, 4028–4035 (2022).
[36]Y. Hu, S. Zhang, Y. Zhu, C. Song, J. Huang, C. Liu, X. Meng, X. Deng, L. Zhu, C. Guan, H. Yang, M. Si, J. Zhang, and Y. Peng, ACS Appl. Mater. Interfaces **14**, 34011 (2022).
[37]S. Bhatti, H. K. Tan, M. I. Sim, V. L. Zhang, M. Sall, Z. X. Xing, R. Juge, R. Mahendiran, A. Soumyanarayanan, S. T. Lim, D. Ravelosona, and S. N. Piramanayagam, APL Mater. **11**, 011103 (2023).
[38]V. Ahrens, C. Kiesselbach, L. Gnoli, D. Giuliano, S. Mendisch, M. Kiechle, F. Riente, and M. Becherer, Adv. Mater. **35**, e2207321 (2023).
[39]G. Yu, P. Upadhyaya, X. Li, W. Li, S. K. Kim, Y. Fan, K. L. Wong, Y. Tserkovnyak, P. K. Amiri, and K. L. Wang, Nano Lett. **16**, 1981 (2016).
[40]S. Yuasa and D. D. Djayaprawira, J. Phys. D: Appl. Phys. **40**, R337–R354 (2007).
[41]M. Ezawa, Phys. Rev. Lett. **105**, 197202 (2010).
[42]M. Heide, G. Bihlmayer, and S. Blügel, Phys. Rev. B **78**(14), 140403 (2008).
[43]Y. Suzuki, S. Miki, Y. Imai, and E. Tamura, Phys. Lett. A **413**, 127603 (2021).
[44]J. F. Ziegler, J. Biersack, and M. D. Ziegler, *SRIM—the Stopping and Range of Ions in Matter* (SRIM, Chester, MD, 2008).

13 March 2024 09:22:49


Published under an exclusive license by AIP Publishing